Journal of ELECTRONIC MATERIALS, Vol. 45, No. 7, 2016
DOI: 10.1007/s11664-016-4517-2
© 2016 The Minerals, Metals & Materials Society

CrossMark

Drop Reliability of Epoxy-contained Sn-58 wt.%Bi Solder Joint with ENIG and ENEPIG Surface Finish Under Temperature and Humidity Test

WOO-RAM MYUNG,[1] YONGIL KIM,[1] KYUNG-YEOL KIM,[2] and SEUNG-BOO JUNG[2,3]

1.—SKKU Advanced Institute of Nanotechnology (SAINT), Sungkyunkwan University, 2066 Seobu-ro, Jangan-gu, Suwon 440-746, South Korea. 2.—School of Advanced Materials Science & Engineering, Sungkyunkwan University, 2066 Seobu-ro, Jangan-gu, Suwon 440-746, South Korea. 3.—e-mail: sbjung@skku.edu

The influence of two kinds of surface finish, namely electroless nickel immersion gold (ENIG) and electroless nickel electroless palladium immersion gold (ENEPIG), on the interfacial reactions and drop reliability of epoxy-enhanced Sn-58 wt.%Bi solder has been investigated after temperature–humidity storage tests. The chemical composition and morphology of intermetallic compounds (IMCs) were characterized by scanning electron microscopy, energy-dispersive x-ray spectroscopy, and electron probe microanalysis. Also, the mechanical reliability of solder joints was evaluated using board-level drop tests. The Sn-Bi epoxy solder/ENEPIG joint exhibited higher IMC growth rate than the Sn-Bi epoxy solder/ENIG joint. After 500 h at 85°C/85% RH storage condition, new IMCs were formed on the Ni_3Sn_4 layer in samples with both surface finishes. The results of board-level drop tests showed that the number of drops was higher for the ENIG than the ENEPIG surface finish. Solder joint fracture occurred along the interface between the solder and IMC layer for the ENIG surface finish. However, with the ENEPIG surface finish, the crack propagated between the IMCs.

Key words: Sn-58 wt.%Bi epoxy solder, ENIG, ENEPIG, board-level drop test, temperature–humidity test

INTRODUCTION

The increased functionality of electronic devices has driven the requirement for smaller, thinner, and multifunctional components. This trend toward miniaturization has been an appreciable challenge to the electronics industry, combined with the conversion to lead-free solders following the regulations on certain hazardous substances (RoHS) and waste electrical and electronic equipment (WEEE).[1,2] The harmful effects of Pb on the environment and health have promoted development of lead-free solders, such as the Sn-Ag, Sn-Cu, Sn-Ag-Cu, and Sn-Bi systems.[3–8] Among them, Sn-Bi alloys are attractive as solder alloys due to their low melting temperature, low cost, and good mechanical properties, such as tensile strength and creep resistance, compared with Sn-Pb alloy.[9–11] In particular, Sn-58 wt.%Bi alloy with eutectic composition has low melting temperature of 138°C, showing that it is possible to reflow at low processing temperature.[12] Low-temperature soldering is necessary because electronic devices are prone to thermal damage during high-temperature reflow processing, which damages not only the solder joints but also the printed circuit board (PCB) and components. Also, low-temperature soldering reduces the risk of warpage problems induced by coefficient of thermal expansion (CTE) mismatch between different materials in the electronic package.[13,14] However, there are some concerns regarding Sn-Bi

(Received July 24, 2015; accepted April 4, 2016; published online April 19, 2016)

alloys, as Bi tends to be brittle.[15] To address this drawback of Sn-Bi alloys, an alternative method is addition of epoxy to Sn-58 wt.%Bi solder.[16–18] In our previous studies, such epoxy-enhanced Sn-58 wt.%Bi solders with organic solderability preservative (OSP) surface finish were examined. The results of shear and drop tests showed that addition of epoxy enhanced the bonding strength of low-melting-temperature/brittle Sn-58 wt.%Bi solder joints.[17,18]

Also, designing for enhanced solder joint reliability is critical to long-lifetime electronic packages, because solder joints are prone to failure in the electronic package under various environmental conditions such as temperature, humidity, dust, shock, and vibration, making it important to evaluate solder joint reliability under harsh environmental conditions.[19,20]

In this work, we demonstrate the effects of two surface finishes, namely electroless nickel immersion gold (ENIG) and electroless nickel electroless palladium immersion gold (ENEPIG), on epoxy-enhanced Sn-58 wt.%Bi solder by means of board-level drop tests to evaluate the mechanical properties of the solder joints under constant temperature–humidity testing.

EXPERIMENTAL PROCEDURES

We investigated the effect of ENIG and ENEPIG surface finishes on the reliability of Sn-58 wt.%Bi epoxy solder by board-level drop tests after constant temperature–humidity treatment for various storage times. Sn-58 wt.%Bi epoxy solder paste (SAM10-401-27, Tamura Co., Japan) containing 14.7% flux with epoxy was employed. To evaluate the thermal behavior of the epoxy and solder, the melting temperature of the epoxy solder paste was measured by differential scanning calorimetry (DSC, Seiko Exstar 6000, Seiko Instruments, Japan). Continuous heating processes were operated at constant heating rate of 5°C/min. The component substrate was a solder mask defined (SMD)-type FR-4 laminate with dimensions of 15 mm × 15 mm × 1 mm with 64 (8 × 8 array) I/O solder pads. The size of the bonding pad opening was 0.38 mm, and the pitch was 1.6 mm. The dimensions of the board substrate were 132 mm × 77 mm × 1 mm, having the same bonding pad configuration as the component substrate. All samples were formed with daisy-chains. To observe the degree of reliability for the different surface finishes, both components and board substrates were prepared with ENIG (5 μm Ni-P and 0.08 μm Au) and ENEPIG (5 μm Ni-P, 0.1 μm Pd, and 0.08 μm Au) surface finishes on Cu bonding pad. Sn-58 wt.%Bi epoxy solder paste was applied by stencil printing on the board substrate. The component substrates were then placed on the board substrate. The reflow process was performed using a reflow machine (RF-430-N2, Japan Pulse Laboratory Co. Ltd., Japan) with peak reflow temperature of 190°C for 5 min. The test samples were then exposed to constant temperature of 85°C with 85% relative humidity (RH) for 100 h, 300 h, 500 h, and 1000 h in a temperature–humidity (TH) test chamber (PL-1KPH, ESPEC CORP., Japan). The board substrate was fixed at the four corners of the drop table of a drop tester (SD-10, LAB, USA) with the mounted packages facing downward. The peak acceleration was 900 G and the pulse duration was 0.7 m/s, in compliance with JESD22-B104-C.[21] To examine the intermetallic compounds (IMCs) formed at the interface of the solder joint as well as the failure mode during the drop test, microstructures and fractured surfaces were observed by scanning electron microscopy (SEM, S-3000H; Hitachi, Japan). The chemical composition of each phase and elemental maps were obtained by energy-dispersive x-ray spectroscopy (EDS, EMAX-7021-H; Horiba, England) and electron probe microanalysis (EPMA, JXA-8500F; JEOL, Japan).

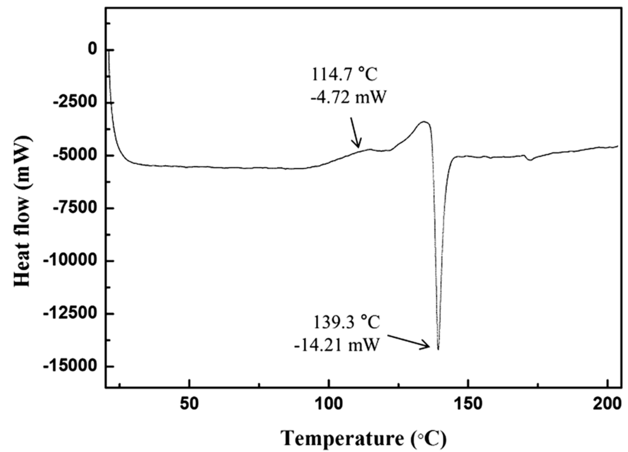

Fig. 1. DSC curve of Sn-58 wt.%Bi epoxy solder paste with heating rate of 5°C/min.

RESULTS AND DISCUSSION

Figure 1 shows the DSC scan obtained at heating rate of 5°C/min. The melting peak of Sn-58 wt.%Bi solder was identified at around 139°C, showing a broad exothermal peak, corresponding to the cross-linking reaction of epoxy at a temperature lower than the melting point of the solder. Figure 2 shows cross-sectional SEM micrographs of the solder joint, as-reflowed and after aging, for the ENIG and ENEPIG surface finishes. The microstructures of Sn-58 wt.%Bi solder consisted of lamellar Bi-rich phase and Sn-rich phase in solder matrix, and the Sn and Bi grains coarsened with increasing aging time in the 85°C/85% RH condition. In the case of the ENIG surface finish, the Au on Ni/Cu pads dissolved rapidly into the solder matrix during reflow and Ni_3Sn_4 IMC was formed by the reaction between Ni of the under bump material (UBM) and

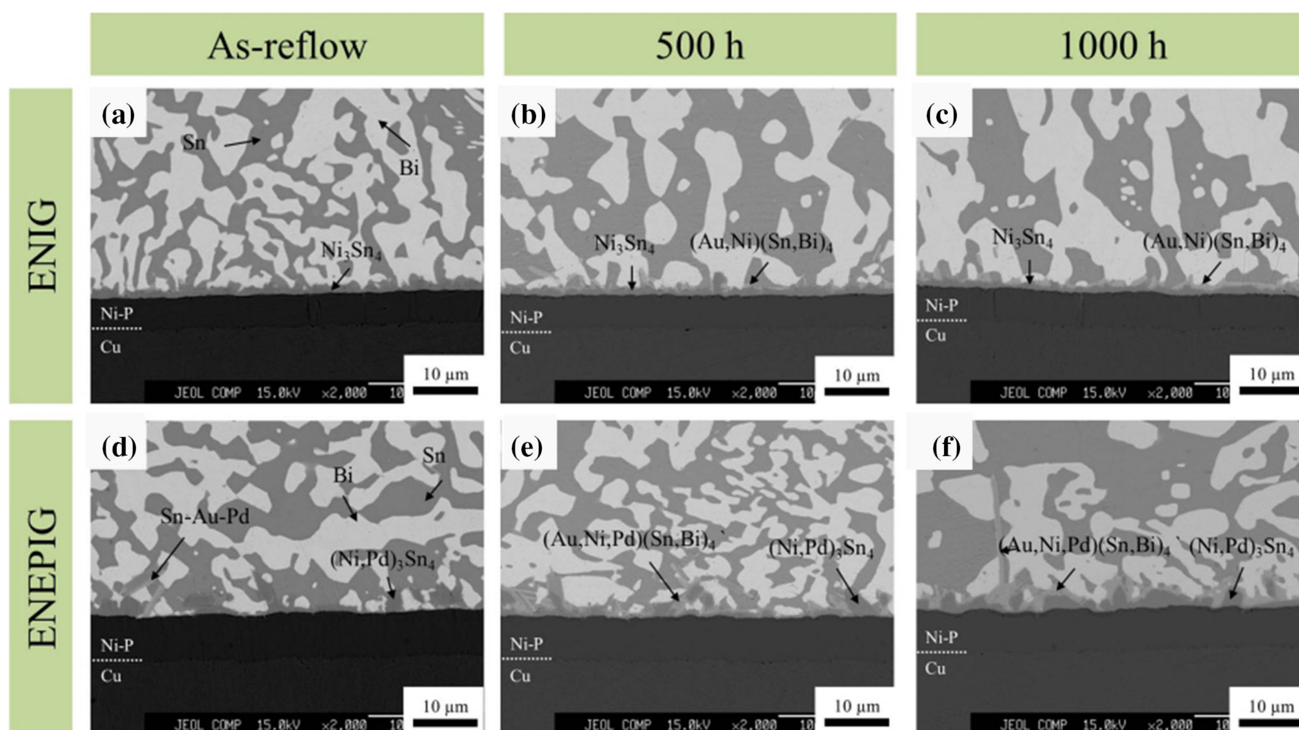

Fig. 2. Cross-sectional SEM micrographs of solder joints: (a, d) as-reflowed, and after aging at 85°C/85% RH condition for (b, e) 500 h and (c, f) 1000 h, for (a–c) ENIG and (d–f) ENEPIG.

Sn in solder.[22] With increasing time, new IMC formed on the Ni_3Sn_4 IMC layer. EDS analysis identified that the chemical composition of the new IMC was approximately 65.35 at.% Sn, 15.95 at.% Bi, 9.20 at.% Ni, and 9.50 at.% Au, corresponding to $(Au,Ni)(Sn,Bi)_4$ phase.[23–25] These IMCs grew with increasing aging time. In the case of the ENEPIG surface finish, the dissolved Au formed Sn-Au-Pd IMCs that precipitated out of the solder during solidification and formed flake-shaped IMCs during reflow. Also, $(Ni,Pd)_3Sn_4$ IMC formed at the interface between the Ni-P layer and Sn-58 wt.%Bi solder. $(Au,Ni,Pd)(Sn,Bi)_4$ IMCs formed on the $(Ni,Pd)_3Sn_4$ IMCs after aging for 500 h. The chemical composition of this IMC was 71.06 at.% Sn, 9.77 at.% Bi, 8.57 at.% Ni, 6.51 at.% Au, and 4.09 at.% Pd. After 1000 h, flake-shaped Sn-Au-Pd IMCs disappeared from the solder during aging, while the thickness of $(Au,Ni,Pd)(Sn,Bi)_4$ and $(Ni,Pd)_3Sn_4$ IMCs increased. It is thought that $(Au,Ni,Pd)(Sn,Bi)_4$ IMC grows by dissolution and deposition of Sn-Au-Pd IMC.[26] The $(Au,Ni,Pd)(Sn,Bi)_4$ IMC did not form after reflow because of the high solubility of Au in the molten solder, causing it to separate from the Ni layer. During aging, subsequent reconfiguration of Au to the interface is known to progress due to the greater thermodynamic stability of the IMC.[27]

Figure 3 shows the variation of the total IMC thickness for solder joints with ENIG and ENEPIG after aging. Both the ENIG and ENEPIG surface finishes showed increasing total IMC thickness with increase of aging time. However, the change of the IMC thickness for the ENIG surface finish during aging was smaller than with the ENEPIG surface finish. The total IMC thickness with the ENIG surface finish increased from about 1.6 μm to 2.1 μm, while with the ENEPIG surface finish it increased from 1.1 μm to 2.9 μm. Less IMCs were formed at the ENEPIG surface finish after reflow due to the limited diffusion reaction between the Ni-P layer and solder caused by the Pd layer. This means that the Pd layer limited Ni diffusion and the reaction between Ni-P and Sn in the solder.[28] On the contrary, the total IMC thickness with ENEPIG was thicker than with ENIG after 1000 h. It is thought that Pd precipitated and formed a new IMC layer with Sn, Bi, Au, and Ni elements during aging, and this IMC grew by thermal effect and reaction of elements.

Figure 4 shows elemental maps for the ENIG surface finish, as-reflowed and after aging for 1000 h. The results indicate that there was little change of the thickness of Ni_3Sn_4 IMC between the as-reflowed state and after aging for 1000 h, and $(Au,Ni)(Sn,Bi)_4$ IMC formed and grew with increasing aging time, so the total IMC thickness increased. It was reported that metastable $(Au,Ni)(Sn,Bi)_4$ IMC nucleated more slowly, but the growth rate of $(Au,Ni)(Sn,Bi)_4$ IMC was faster than that of Ni_3Sn_4 IMC.[29,30] Thus, the total IMC thickness with the ENIG surface finish was governed by $(Au,Ni)(Sn,Bi)_4$ IMC rather than Ni_3Sn_4 IMC. In the case of the ENEPIG surface finish, as shown in Fig. 5, the

thickness of $(Ni,Pd)_3Sn_4$ IMC increased with increasing aging time. Also, irregular $(Au,Ni,Pd)(Sn,Bi)_4$ IMC with whiskers formed and grew on the $(Ni,Pd)_3Sn_4$ IMC during aging. As a result, the total IMC thickness with the ENEPIG surface finish was greater than with the ENIG surface finish, because two types of IMC grew with increasing aging time. Also, carbon from the epoxy content was not observed in the solder joints.

Figure 6 presents SEM micrographs showing top views of etched IMC morphologies for Sn-58 wt.%Bi epoxy solder/ENIG and ENEPIG joints, as-reflowed and after aging time of 1000 h. From these top-view micrographs, facet-shaped Ni_3Sn_4 IMC was observed in Sn-58 wt.%Bi epoxy solder/ENIG joints under the reflow process. The IMC morphology changed to needle shape, and the size of the IMC became larger after aging for 1000 h, because of the formation of new IMC by precipitation of Au. For the ENEPIG surface finish, only needle-shaped $(Ni,Pd)_3Sn_4$ IMC formed at the interface after reflow, as shown in Fig. 6c. There was no shape change after 1000 h, although the IMC surface was rougher and the chemical composition of the IMC changed to $(Au,Ni,Pd)(Sn,Bi)_4$, as shown in Fig. 2f. According to these results, the IMC morphology was affected by the type of surface finish. In other words, in the case of the ENIG surface finish, the IMC morphology was facet shaped and the size of the IMC was below 5 μm after reflow. After aging time of 1000 h, both facet- and needle-shaped IMCs were observed on the ENIG surface finish, and these IMCs grew over 5 μm. On the other hand, the IMC formed on the ENEPIG surface showed needle-shape morphology with length of more than 10 μm. Also, the IMC morphology did not change much with aging time.

Figure 7 shows the average number of drops of Sn-58 wt.%Bi epoxy solder joints for the different surface finishes. Sn-58 wt.%Bi solder joints without epoxy addition failed at fewer than 10 drops regardless of the surface finish.[17] However, the drop reliability of Sn-58 wt.%Bi epoxy solder joints was enhanced in comparison with Sn-58 wt.%Bi solder joints. The average number of drops for Sn-58 wt.%Bi epoxy solder/ENIG and ENEPIG was 46

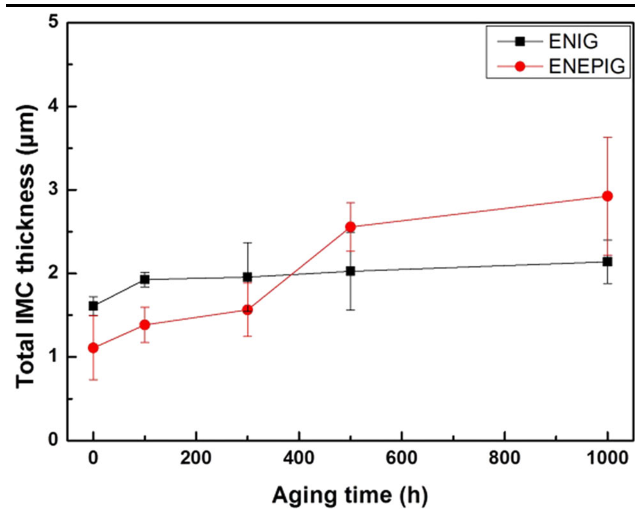

Fig. 3. Total IMC thickness with aging time at 85°C/85% RH condition.

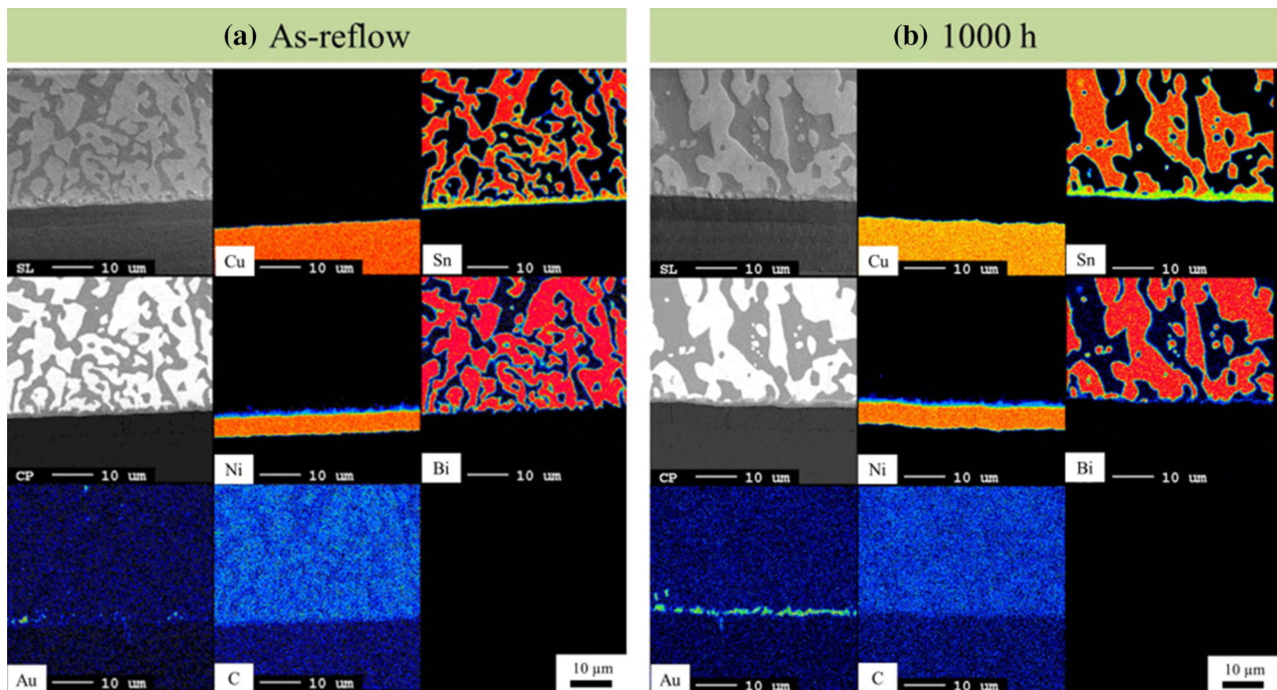

Fig. 4. EPMA analysis of ENIG surface finish (a) after reflow and (b) aging at 85°C/85% RH condition for 1000 h.

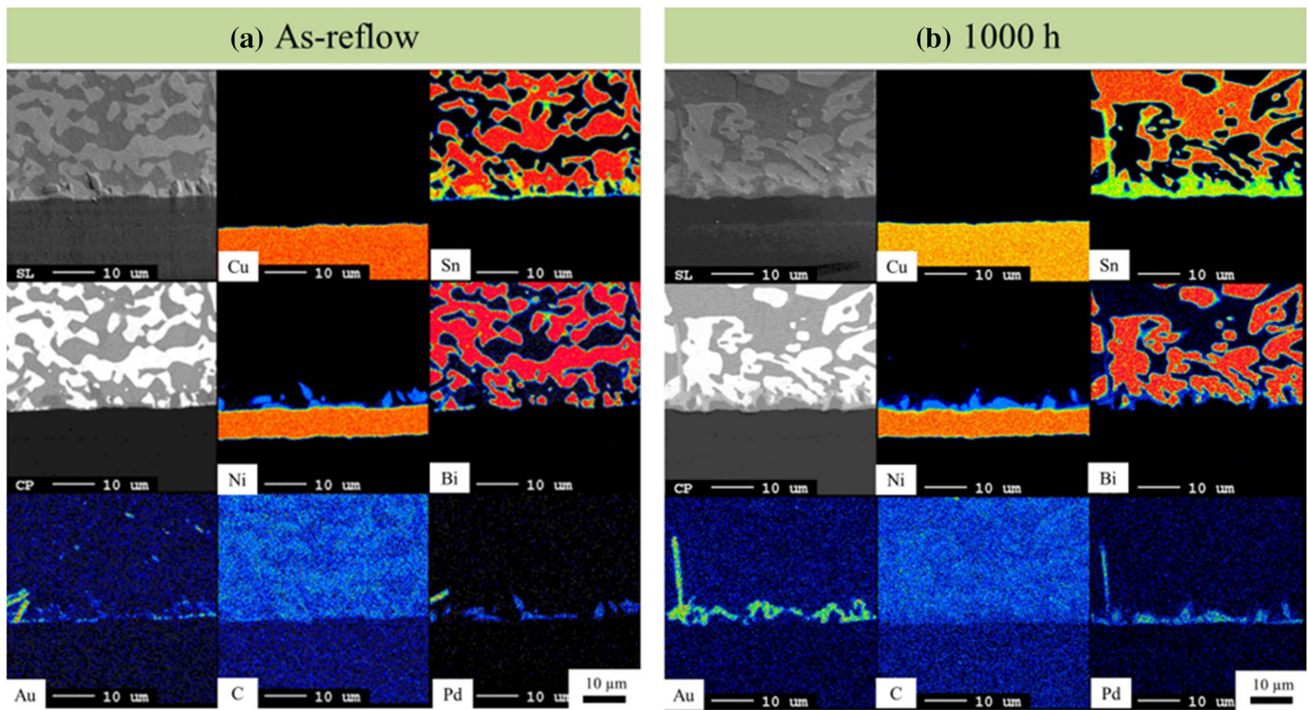

Fig. 5. EPMA analysis of ENEPIG surface finish (a) after reflow and (b) aging at 85°C/85% RH condition for 1000 h.

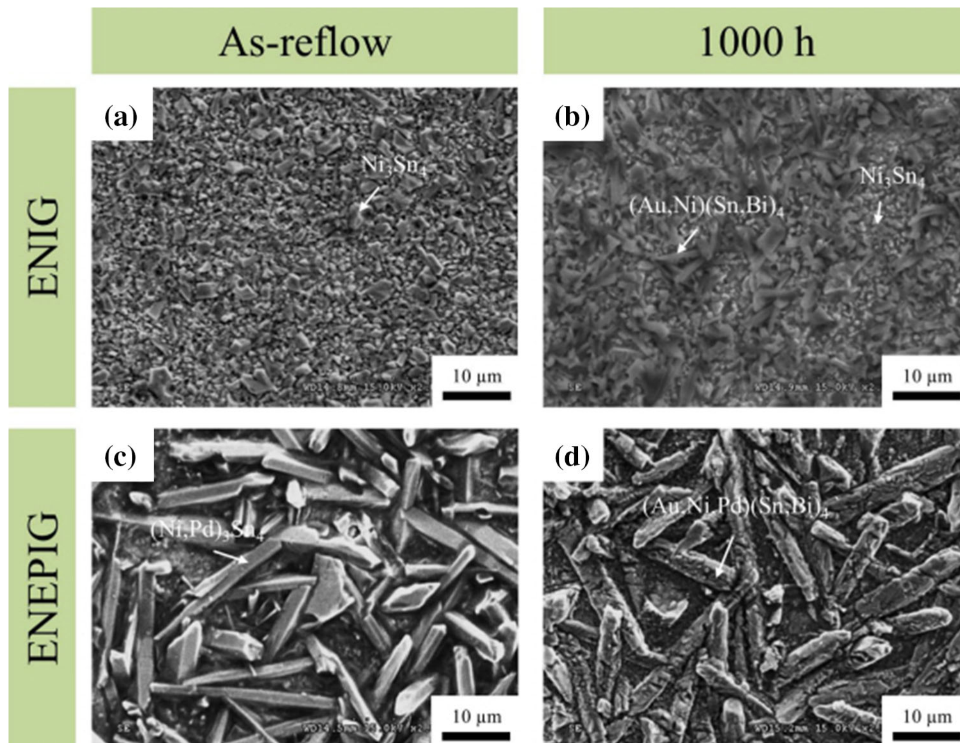

Fig. 6. SEM micrographs showing top views of IMCs after preferential etching: (a, c) as-reflowed and (b, d) after aging at 85°C/85% RH condition for 1000 h.

and 63, respectively. The drop reliability of Sn-58 wt.%Bi epoxy solder joints decreased with increasing aging time at the 85°C/85% RH condition. The number of drops without failure for the Sn-58 wt.%Bi epoxy solder/ENEPIG joints was higher than for the Sn-58 wt.%Bi epoxy solder/

ENIG joints after the reflow process. It was thought that this result was related to the IMC formation and its thickness in the solder joints. Generally, the thickness of the IMC layer is known to be a governing factor determining solder joint reliability because an excessively thick IMC layer is sensitive to stress, and provides initiation sites and paths for crack propagation.[31,32] The variation in the total IMC thickness for the ENEPIG surface finish was greater than for the ENIG surface finish. Also, the total number of drops without failure for the ENIG and ENEPIG surface finishes decreased by 69% and 94%, respectively. This means that cracking easily occurred at a thicker IMC layer with increased aging at the 85°C/85% condition.

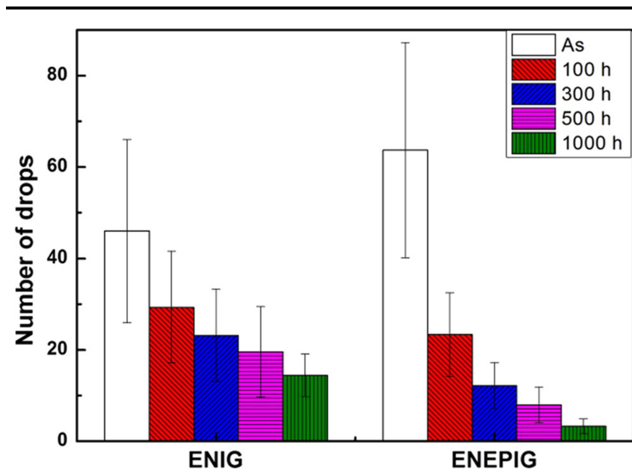

Fig. 7. Number of drops of Sn-58 wt.%Bi epoxy solder joints.

Figure 8 shows the failure of Sn-58 wt.%Bi epoxy solder/ENIG and ENEPIG joints after aging in the 85°C/85% condition for 0 h, 500 h, and 1000 h, followed by board-level drop testing. The crack for the ENIG surface finish was observed at the interface between the Ni_3Sn_4 IMC and Ni-P layer for the as-reflowed sample. The results for solder joints subjected to aging for 500 h and 1000 h are shown in Fig. 8b and c. A dominant crack can be seen at the interface between $(Au,Ni)(Sn,Bi)_4$ IMC and solder, while some inclined minor cracks extended to Bi-rich grains in the solder after aging for 1000 h. These minor cracks stopped at Sn-rich grains in the solder. However, a different failure mode was observed for the ENEPIG surface finish, as shown in Fig. 8d–f. The crack occurred mostly inside the solder after reflow, and the crack path was irregular. After 500 h of aging, a crack occurred in the interface between $(Au,Ni,Pd)(Sn,Bi)_4$ IMC and solder, propagating along the IMC layer. After 1000 h of aging, the crack path was located close to the $(Ni,Pd)_3Sn_4$ IMC/Ni-P interface, where the $(Au,Ni,Pd)(Sn,Bi)_4$ IMC layer developed during the aging test.

Figure 9 shows the paths of the cracks at the epoxy side, where it can be seen that there are two types of fracture mode. In one, the crack initiated in the middle of the epoxy side and propagated at the interface between the epoxy and solder ball. In the other, the crack initiated at the end of the epoxy

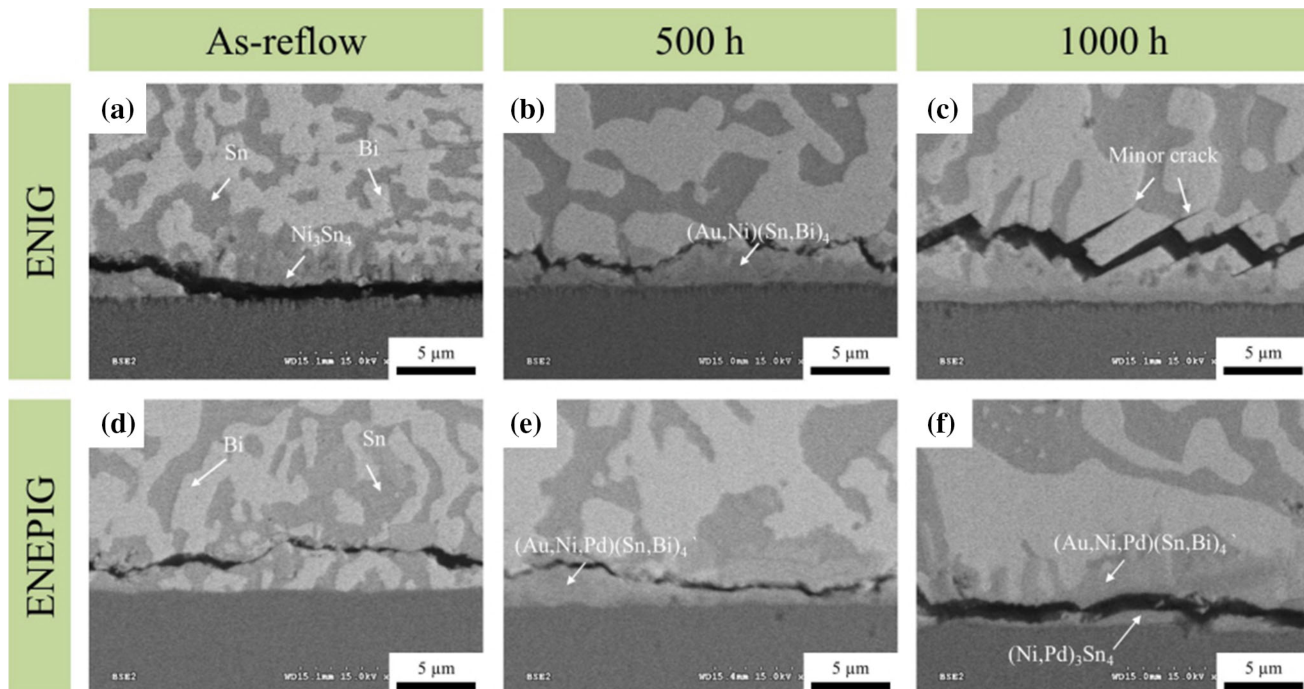

Fig. 8. Cross-sectional SEM micrographs after drop test: (a, d) as-reflowed, and with aging at 85°C/85% RH condition for (b, e) 500 h and (c, f) 1000 h, for (a–c) ENIG and (d–f) ENEPIG.

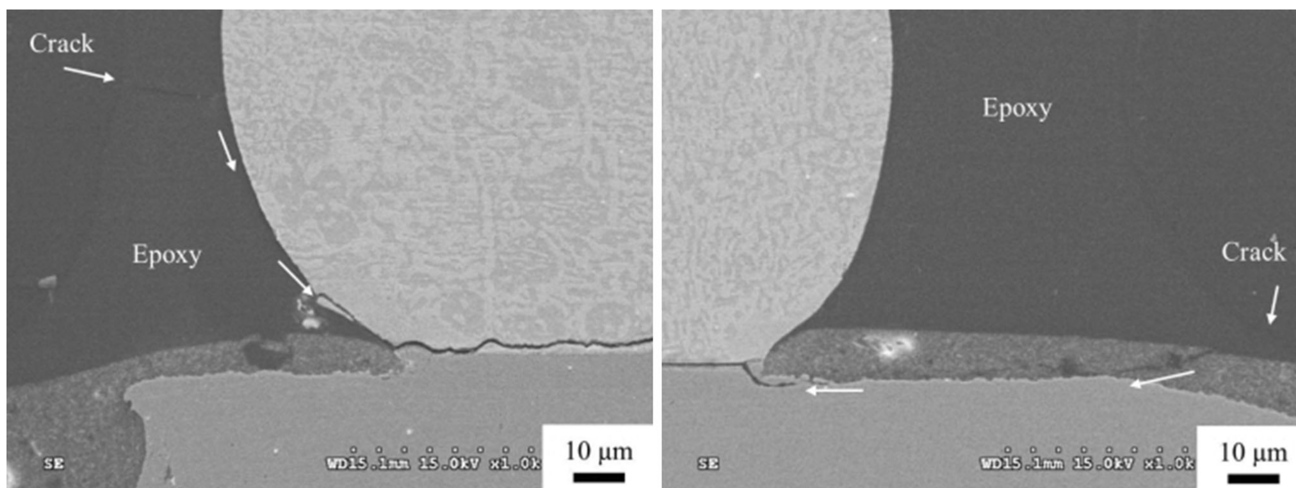

Fig. 9. Cross-sectional SEM micrographs of crack propagation after drop test.

side on the substrate and spread across the inside of the substrate.

CONCLUSIONS

We investigated the interfacial reaction and drop reliability of Sn-58 wt.%Bi epoxy solder with ENIG or ENEPIG surface finish after aging at 85°C/85% RH for various times. Ni_3Sn_4 IMC was formed by reaction between Sn in the solder and Ni in the ENIG surface finish after the reflow process. With increasing aging time, $(Au,Ni)(Sn,Bi)_4$ IMC formed on the Ni_3Sn_4 IMC layer. $(Ni,Pd)_3Sn_4$ IMC formed at the interface between the ENEPIG surface finish and solder. Also, $(Au,Ni,Pd)(Sn,Bi)_4$ IMCs formed on the Ni_3Sn_4 IMC after 500 h. Overall, the total IMC thickness increased with increasing aging time. However, the change of the IMC thickness with the ENEPIG surface finish during aging was larger than for the ENIG surface finish after 300 h. The IMC morphology with the ENIG surface finish changed from faceted to needle shape. However, the IMC morphology with the ENEPIG surface finish showed typical needle shape after aging at the 85°C/85% RH condition. The drop reliability of Sn-58 wt.%Bi epoxy solder joints decreased with increasing aging time, and the number of drops without failure of the Sn-58 wt.%Bi epoxy solder/ENIG joints was higher than that of Sn-58 wt.%Bi epoxy solder/ENEPIG joints. The crack propagation with the ENIG surface finish changed from between the Ni_3Sn_4 IMC and Ni-P layer to between the $(Au,Ni)(Sn,Bi)_4$ IMC and solder. However, the crack with the ENEPIG surface finish mainly initiated within the solder, propagating between the $(Ni,Pd)_3Sn_4$ IMC and $(Au,Ni,Pd)(Sn,Bi)_4$ IMC after aging for 500 h.

ACKNOWLEDGEMENTS

This work was supported by the Human Resources Program in Energy Technology of the Korea Institute of Energy Technology Evaluation and Planning (KETEP) granted financial resource from the Ministry of Trade, Industry, & Energy, Republic of Korea (20154030200870).

REFERENCES

1. P. Cox and G. Drys, Report No. Directive 2002/95/EC, Official Journal of the European Union, Brussels, January 2003.
2. P. Cox and G. Drys, Report No. Directive 2002/96/EC, Official Journal of the European Union, Brussels, January 2003.
3. Q. Zhao, J. Bi, A. Hu, M. Li, and D. Mao, in *International Conference on Electronic Packaging Technology & High Density Packaging* (2012), pp. 1226–1229. doi:10.1109/ICEPT-HDP.2012.6474827.
4. W.M. Chen, S.K. Kang, and C.R. Kao, *J. Alloys Compd.* 520, 244 (2012).
5. J.W. Yoon, S.W. Kim, J.M. Koo, D.G. Kim, and S.B. Jung, *J. Electron. Mater.* 33, 1190 (2004).
6. L.C. Shiau, C.E. Ho, and C.R. Kao, *Solder. Surf. Mt. Technol.* 14, 25 (2002).
7. C.Z. Liu and W. Zhang, *J. Mater. Sci.* 44, 149 (2009).
8. J.W. Yoon, B.I. Noh, B.K. Kim, C.C. Shur, and S.B. Jung, *J. Alloys Compd.* 486, 142 (2009).
9. J. Wang, H.S. Liu, L.B. Liu, and Z.P. Jin, *J. Electron. Mater.* 35, 1842 (2006).
10. J.W. Yoon, C.B. Lee, and S.B. Jung, *Mater. Trans.* 43, 1821 (2002).
11. P.L. Liu and J.K. Shang, *J. Mater. Res.* 16, 1651 (2001).
12. M.S. Suh, C.J. Park, and H.S. Kwon, *Surf. Coat. Technol.* 200, 3527 (2006).
13. Q.K. Zhang and Z.F. Zhang, *Mater. Sci. Eng. A.* 528, 2686 (2011).
14. M.C. Liao, P.S. Huang, Y.H. Lin, C.Y. Huang, M.Y. Tsai, and T.C. Huang, in *International Microsystems, Packaging, Assembly and Circuits Technology Conference* (2014), pp. 397–400. doi:10.1109/IMPACT.2014.7048436.
15. B. Sandy, E. Briggs, R. Lasky, Indium Corporation Tech Paper, 1 (2011). http://www.indium.com/techlibrary/whitepapers/advantages-of-bismuthbased-alloys-for-low-temperature-pbfree-soldering-and-rework. Accessed 27 June 2014.
16. I. Cho, J.H. Ahn, J.W. Yoon, Y.E. Shin, and S.B. Jung, *J. Mater. Sci.* 23, 1515 (2012).
17. W.R. Myung, Y. Kim, and S.B. Jung, *J. Alloys Compd.* 615, S411 (2014).

18. J. Kim, W.R. Myung, and S.B. Jung, *J. Microelectron. Packag. Soc.* 21, 97 (2014).
19. L. Zhang, J.G. Han, C.W. He, and Y.H. Guo, *J. Mater. Sci.* 24, 172 (2013).
20. S.G. Desmarest, *Mater. Sci. Tech-lond.* 28, 257 (2012).
21. JEDEC Solid State Technology Association, JESD22-B104C "Mechanical Shock", 2004.
22. J.W. Yoon, C.B. Lee, and S.B. Jung, *Mater. Trans.* 43, 1821 (2002).
23. L.T. Chen and C.M. Chen, *J. Mater. Res.* 21, 962 (2006).
24. M.G. Cho, K.W. Paik, H.M. Lee, S.W. Booh, and T.G. Kim, *J. Electron. Mater.* 36, 35 (2006).
25. C.C. Chi, L.C. Tsao, C.W. Tsao, and T.H. Chuang, *J. Mater. Eng. Perform.* 17, 134 (2008).
26. Z. Mei, M. Kaufmann, A. Eslambolchi, and P. Johnson, in *Electronic Components and Technology Conference* (1998), pp. 952–961.
27. A.M. Minor and J.W. Morris Jr., *J. Electron. Mater.* 29, 1170 (2000).
28. S.S. Ha, J. Park, and S.B. Jung, *Mater. Trans.* 52, 1553 (2011).
29. C.M. Chen and S.W. Chen, *J. Mater. Res.* 18, 1293 (2003).
30. C. Fuchs, T. Schreck, and M. Kaloudis, *J. Mater. Sci.* 47, 4036 (2012).
31. D. Yao and J.K. Shang, *Metall. Mater. Trans. A* 26, 2677 (1995).
32. Y.C. Chan, P.L. Tu, C.W. Tang, K.C. Hung, and J.K.L. Lai, *IEEE Trans. Adv. Packag.* 24, 25 (2001).